JOURNAL OF GEOPHYSICAL RESEARCH, VOL. 107, NO. A8, 1154, 10.1029/2001JA007550, 2002

Solar cycle changes in coronal holes and space weather cycles

J. G. Luhmann,[1] Y. Li,[1] C. N. Arge,[2] P. R. Gazis,[3] and R. Ulrich[4]

Received 17 August 2001; revised 21 December 2001; accepted 21 December 2001; published 1 August 2002.

[1] Potential field source surface models of the coronal magnetic field, based on Mt. Wilson Observatory synoptic magnetograms, are used to infer the coronal hole sources of low-heliolatitude solar wind over approximately the last three solar cycles. Related key parameters like interplanetary magnetic field and bulk velocity are also calculated. The results illustrate how the evolving contribution of the polar hole sources relative to that from low-latitude and midlatitude active region hole sources can explain solar magnetic field control of long-term interplanetary variations. In particular, the enduring consistent magnetogram record and continuous model displays produce a useful overview of the solar control of interplanetary cycles and trends that affect space weather. *INDEX TERMS:* 2169 Interplanetary Physics: Sources of the solar wind; 2164 Interplanetary Physics: Solar wind plasma; 2162 Interplanetary Physics: Solar cycle variations (7536); *KEYWORDS:* solar wind sources, coronal holes, solar cycle

1. Introduction

[2] Space weather depends not only on the transient interplanetary disturbances from coronal mass ejections (CMEs) but also on the ambient solar wind flows and fields. The majority of the time, even during solar maximum, key interplanetary parameters, including plasma bulk speed and magnetic field strength and orientation, are controlled by the characteristics of the prevailing coronal holes [cf. *Wang and Sheeley*, 1994]. These ambient solar wind conditions also influence the geomagnetic activity consequences of CMEs by affecting their propagation speed, the interplanetary field and dynamic pressure in the compressed region preceding the ejecta, and the distortion of the ejecta in the nonuniform solar wind stream structure [e.g., *Riley et al.*, 1997; *Odstrcil and Pizzo*, 1999]. Thus interpretations of space weather and geomagnetic activity trends in terms of solar changes [e.g., *Lockwood et al.*, 1999; *Stamper et al.*, 1999] require a clear picture of the sources of the ecliptic solar wind through the solar cycle.

[3] Over 20 years ago, *Levine* [1978, 1982] and others had demonstrated the ability of potential field source surface models of the coronal magnetic field to reproduce coronal hole foot points at the photosphere seen in He10830 angstrom images throughout the solar cycle, as well as to explain some high-speed streams detected at Earth during the disk passage of certain coronal hole features. Since then, *Wang and Sheeley* [1990a, 1994] have undertaken a number of studies of the long-term solar magnetic field control of coronal holes and solar wind using potential field source surface models based on Mt. Wilson Observatory magnetograph records. One of the important points of these earlier results is that the tilted dipole axis/polar coronal hole source model often used to describe the solar cycle variation of the solar wind and as a pedagogical tool [e.g., *Zhao and Hundhausen*, 1981] can be misleading. Instead, they showed that the polar holes become less important as the solar cycle progresses. As soon as new active regions emerge, the ecliptic solar wind sources begin a transition from the polar holes to a combination of polar coronal hole extensions and isolated low-latitude holes associated with the active regions. The distortion of the polar coronal holes by large active region complexes causes the neutral line on the source surface to become increasingly inclined (with respect to the equator) on the approach to solar polarity reversal. The main polar holes remain at high latitudes on the photosphere, shrinking as the cycle progresses. The low-latitude holes and polar coronal hole extension sources provide a natural explanation for the complex low-latitude solar wind observed in interplanetary scintillation (IPS) measurements [e.g., *Asai et al.*, 1998; *Kojima et al.*, 1999] and by Ulysses [*McComas et al.*, 2000; *von Steiger et al.*, 2000], though it is likely that there is also a contribution to low-latitude solar wind from weak coronal transients associated with the edges of the helmet streamer belt [*Crooker et al.*, 1993, 1996; *Sheeley et al.*, 1999].

[4] In a recent effort to identify specific sources of the solar wind observed by spacecraft upstream of Earth, *Neugebauer et al.* [1998] found that the coronal holes inferred from the potential field source surface model agree well with the corresponding results from three-dimensional MHD models of the corona, at least for periods of modest solar activity. Their conclusion relevant to the present study is that the solar wind observed by the Wind spacecraft during Carrington rotations 1892–1894 in early 1995 originated from a combination of flows from low-latitude

[1]Space Sciences Laboratory, University of California, Berkeley, California, USA.
[2]CIRES, University of Colorado, and NOAA Space Environment Center, Boulder, Colorado, USA.
[3]NASA Ames Research Center, Moffet Field, California, USA.
[4]Department of Physics and Astronomy, University of California, Los Angeles, California, USA.

0148-0227/02/2001JA007550$09.00

coronal holes and the edges of the polar coronal holes, including their low-latitude extensions. At this time the solar magnetic field was nearly dipolar with only a few active regions on the disk, producing a modestly warped, nearly equatorial heliospheric current sheet. The inferred contribution of the polar hole edge flows to the ecliptic wind was ~50%.

[5] In this paper we apply a similar approach to infer the low heliospheric latitude solar wind sources during, approximately, the past three solar activity cycles, a period covering Carrington rotations 1600–1965 (roughly, April 1973 through August 2000). As in the work of *Wang et al.* [2000], the archive of synoptic maps from the Mt. Wilson Observatory magnetograph [*Ulrich*, 1992] is used to provide the inner boundary conditions for potential field source surface models of the coronal magnetic field. Both estimated coronal hole patterns and coronal hole associations of the low-latitude solar wind are derived over this time, for which fairly continuous upstream solar wind measurements are also available. The results provide insight into the solar magnetic field control of solar wind properties that affect Earth and suggest how it modulates the cycles observed in solar wind parameters and space weather.

2. Construction of Synoptic Maps From Mt. Wilson

[6] Line-of-site (LOS) photospheric field measurements of the Sun have been made at Mt. Wilson Solar Observatory (MWO) since 1966 and are presently available in the MWO computer archive in the form of full Carrington maps. The LOS photospheric field strength is measured at MWO using the Fe I 525.0 nm line in the solar spectrum. However, *Ulrich* [1992] demonstrated that magnetic field strength derived from this line must be modified by a correction factor due to line saturation effects. This correction factor depends both on the spatial resolution of the instrument and the center-to-limb position of the observation and was determined by comparing photospheric field strengths derived from the Fe I 525.0 nm line to those derived from the Fe I 523.3 nm line, which does not saturate. For data taken with large apertures such as with MWO, *Ulrich* [1992] determined that the empirical correction factor for the Fe I 525.0 nm line depends only on the center-to-limb angle. Carrington maps of the LOS field are constructed so that they are weighted most heavily about observations made near central meridian; thus the center-to-limb angle can be replaced with the heliographic latitude (λ). This approach is identical to that taken by *Wang and Sheeley* [1995] and results in the following empirical correction factor for the Fe I 525.0 nm line: $F = 4.5 - 2.5 \sin 2(\lambda)$. We apply this factor to the set of Carrington maps used in this study, as MWO has yet to correct their maps for line saturation effects.

[7] Observational evidence [*Wang and Sheeley*, 1992] suggests that the solar magnetic field is nearly radial at the photosphere. Assuming that the magnetic field is truly radial in the region of the photosphere where the measurements are taken, the relationship between the radial field (B_r) and the LOS field (B_{LOS}) is $B_r = B_{LOS}/\cos(\lambda - b)$, where the solar b angle is the apparent tilt of the Sun's rotation axis as viewed from Earth. MWO's archived set of Carrington maps are for the LOS field and therefore require conversion to radial orientation. This is achieved by simply dividing the data by the factor $\cos(\lambda - b)$. We interpolate the MWO Carrington maps, originally in sine latitude format, to a uniform $360^\circ \times 180^\circ$ grid with $5^\circ \times 5^\circ$ cell sizes. Since the Carrington maps are not true synoptic maps (i.e., the data are not taken all at the same instant), they usually have a small monopole moment that requires removal. To ensure that $\nabla \cdot B = 0$, each map's monopole moment was calculated and then uniformly subtracted from it. Carrington maps with large data gaps are not used, and those with small gaps are filled.

[8] As mentioned above, the set of MWO Carrington maps used in this study are from Carrington rotations (CRs) 1600 (roughly, April 1973) through CR 1965 (roughly, August 2000). Complete Carrington maps exist as far back as CR 1517 (1966) at MWO. However, we chose to begin with CR 1600 since Kitt Peak Solar Observatory Carrington maps also exist back to nearly CR 1600. Comparison of the maps from both observatories (not shown here) show reasonable agreement and provide additional confidence in the quality of the MWO maps from CR 1600 to the present, although problems with both the MWO and Kitt Peak LOS data from CR 1600 to the present are known to exist. For instance, the magnetograph used at MWO in the 1980s seems to have generated weaker than normal field values and Kitt Peak polar fields are problematic before about CR 1992.

3. Potential Field Source Surface Model

[9] We adopt the standard potential field source surface (PFSS) model approach, in which solutions of Laplace's equation in terms of spherical harmonic expansions are obtained using the observed photospheric magnetic field as the inner boundary condition [e.g., *Schatten et al.*, 1969; *Altschuler and Newkirk*, 1969]. On the basis of earlier studies aimed at optimizing the PFSS model for use in coronal hole and interplanetary magnetic field polarity studies [e.g., *Hoeksema et al.*, 1983; *Wang*, 1993; *Zhao and Hoeksema*, 1995a, 1995b], we assume that the observed photospheric field is radial, use a 2.5 solar radius source surface, and include 17 orders of the harmonic coefficients derived from the solution to calculate the coronal magnetic field.

[10] Shortcomings of the PFSS approach include its neglect of coronal currents and the nonpotential nature of some active regions and the use of a spherical source surface that constrains the coronal field to become radial at a specified altitude regardless of location. Although a few studies have used nonspherical source surfaces, they have been restricted to special cases because realistic multipolar field boundary conditions present computational challenges [e.g., *Levine et al.*, 1982; *Schulz*, 1997]. There are also corrections that can be made to the PFSS model to better represent the effects of the heliospheric current sheet on the field geometry [e.g., *Zhao and Hoeksema*, 1995a; *Wang and Sheeley*, 1995], but we also neglect this complication in our coronal hole oriented study. Finally, the synoptic maps, whose construction is described in section 2, do not represent true snapshots of the global

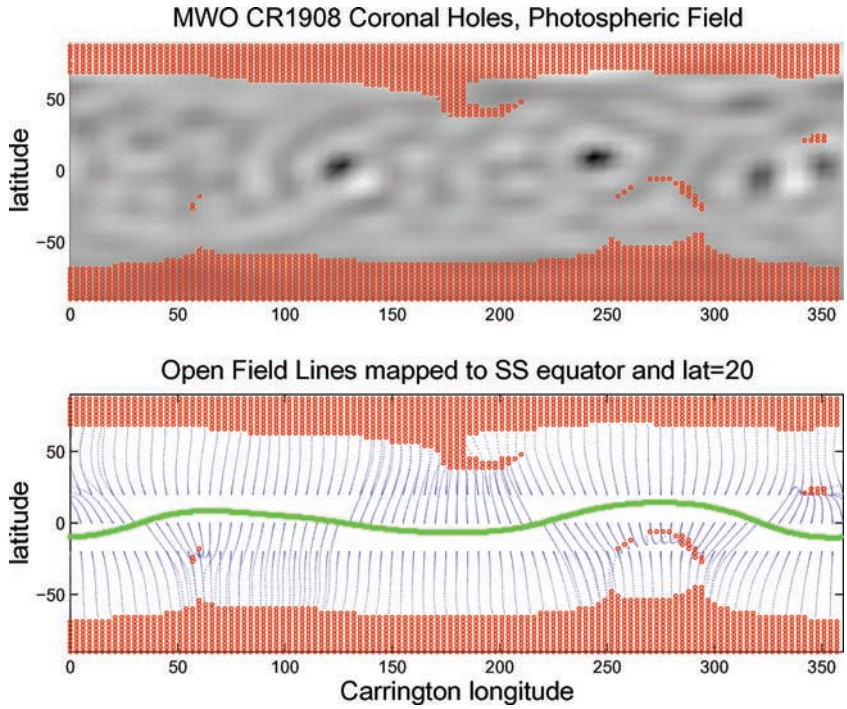

Figure 1a. Illustration of the approach to mapping from the low-latitude source surface, along potential field source surface model coronal field lines, and back to their source in the photosphere. This Carrington rotation (CR) represents an example from near solar minimum when the polar coronal holes dominate the inferred source of the near-ecliptic solar wind. MWO stands for Mt. Wilson Observatory.

photospheric field. Thus, especially around solar maximum when the photospheric magnetic field significantly changes on timescales faster than the solar rotation period of ~27 days, the derived coronal field structure departs from the actual structure. Nevertheless, previous tests of the observation-based PFSS model provide confidence in its ability to give generally good approximations of coronal hole behavior throughout the solar cycle [e.g., *Levine*, 1982].

4. Modeled Coronal Hole Sources

[11] Figures 1a–1c illustrate three sample Carrington rotations for quiet, moderate, and active solar field conditions. The top panels of each plot include a contour map of the observed photospheric field in Carrington coordinates, smoothed to emphasize large-scale features, with the open field regions calculated from the superimposed PFSS model. The grayscale of the contour maps indicates radial field strength and direction, with black representing the strongest inward pointing fields and white representing the strongest outward pointing fields. The red dotted areas indicate the locations on the photosphere where the foot points of PFSS model field lines connect to the source surface at 2.5 solar radii. The bottom panels include the same open field regions, together with the projections of coronal field lines intercepting the low-latitude source surface at the equator, and 20°N and 20°S latitudes. *Levine* [1978] used similar displays to describe the sources of the upstream solar wind, assuming that the coronal field lines reaching the source surface equator represent effective stream tubes. The heavy line is the projection of the source surface neutral line that separates solar wind streams of opposite magnetic polarity.

[12] The example in Figure 1a, for the quiet Sun, shows the classical picture of ecliptic solar wind from the edges of the polar holes, giving a few well-defined magnetic sectors arising from the Northern and Southern Hemispheres. As the number of important active regions increases, this picture evolves to that in Figure 1b, where the low-latitude solar wind sources begin to detach from the polar coronal holes even though they remain a dominant feature. At such times the solar wind in the heliosphere must include contributions from the different coronal hole sources in the polar quiet Sun and the more active midlatitudes. The picture in Figure 1c illustrates the situation when the polar holes have vanished, leaving the active region holes to supply the solar wind throughout the heliosphere.

[13] The long-term versions of these plots are constructed by reversing the Carrington longitude axes to effectively represent time (Carrington time) and by then merging a sequence of consecutive plots end to end into a continuous display that can be thought of as a picture of coronal hole evolution as seen on the central meridian. This time series, running from roughly April 1973 to August 2000, is then broken into three segments that allow the trends to be compared for approximately three solar cycles (21, 22, and 23). Figure 2 contains plots of the sunspot number in

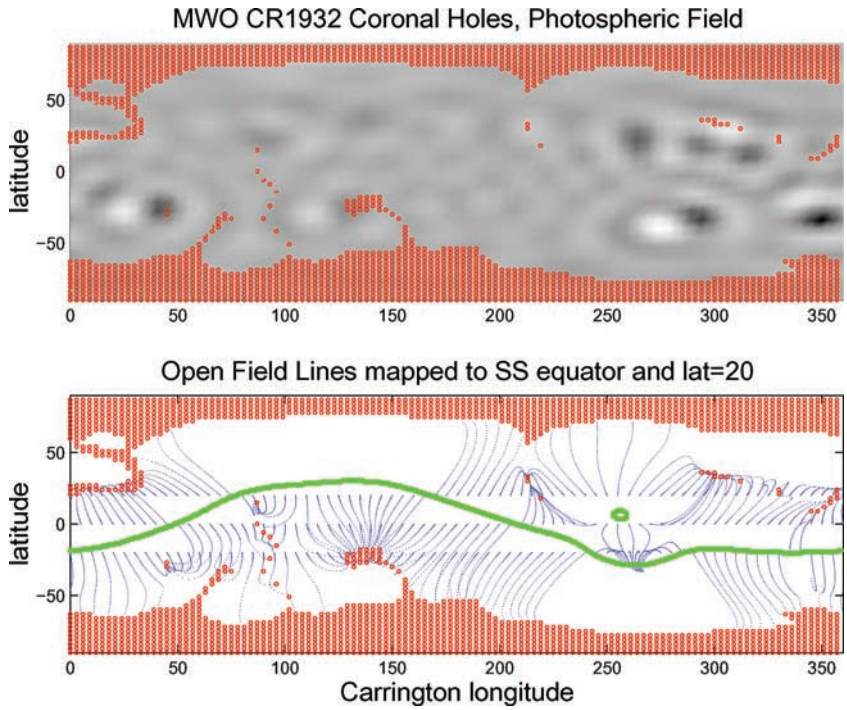

Figure 1b. Same as Figure 1a but for a Carrington rotation, for which the inferred low-latitude solar wind source was divided between the edges of the polar coronal holes, polar hole extensions, and several isolated low-latitude coronal holes. This case represents the pattern found over most of the solar cycle, during both rising and declining phases.

the same general layout to guide the viewer in interpreting the model displays. As shown here, each segment extends from just presolar minimum through the beginning of the declining phase of the cycle (except for cycle 23).

[14] Figure 3 contains the long-term picture of the photospheric field open regions or coronal holes, as represented by the PFSS model. The polar holes disappear only for a brief period around solar maximum, when the

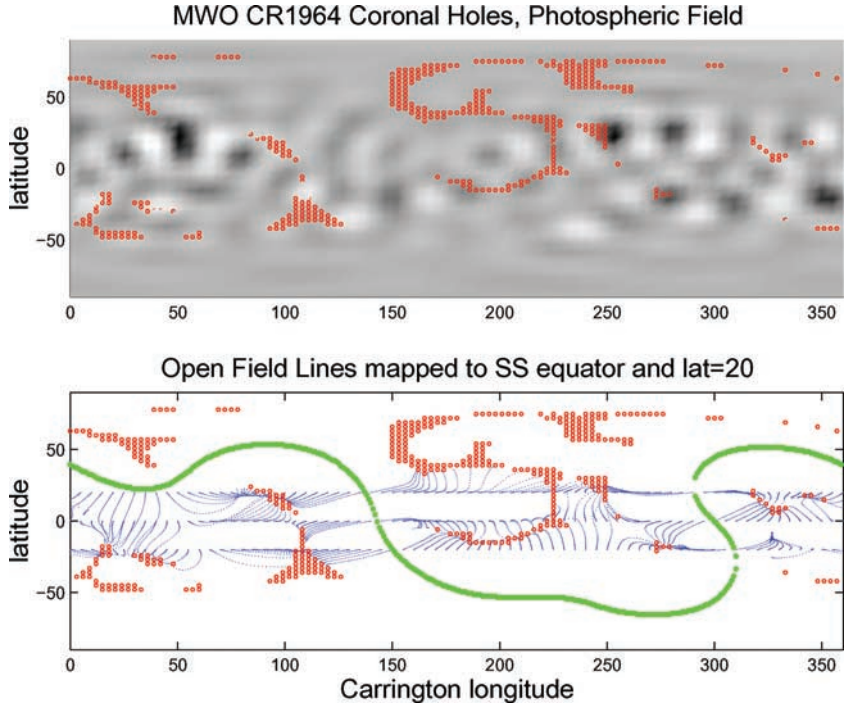

Figure 1c. Same as Figures 1a and 1b but for a Carrington rotation for which the inferred low-latitude solar wind source was restricted to several isolated low-latitude coronal holes. This situation is found only for a brief interval around solar maximum, when the polar holes are absent.

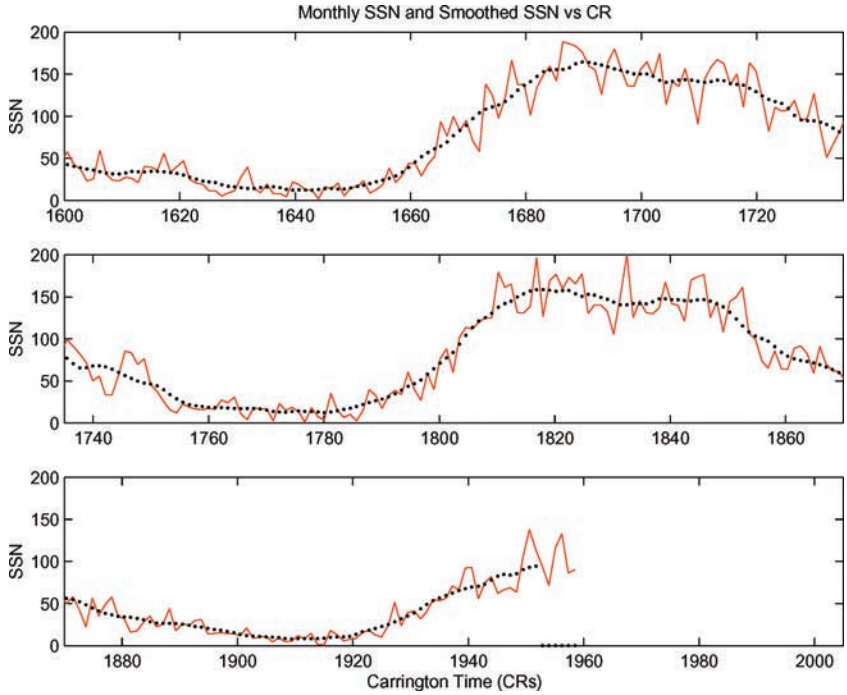

Figure 2. Monthly sunspot numbers (SSNs; from the National Solar Observatory-Kitt Peak) for the period analyzed. The included Carrington rotations starting in April 1973 and lasting until June 2000. The dates covered in each panel are: (top) April 1973 (CR 1600) to May 1983 (CR 1735), (middle) May 1983 (CR 1735) to June 1993 (CR 1870), and (bottom) June 1993 (CR 1870) to July 2000 (CR 1965).

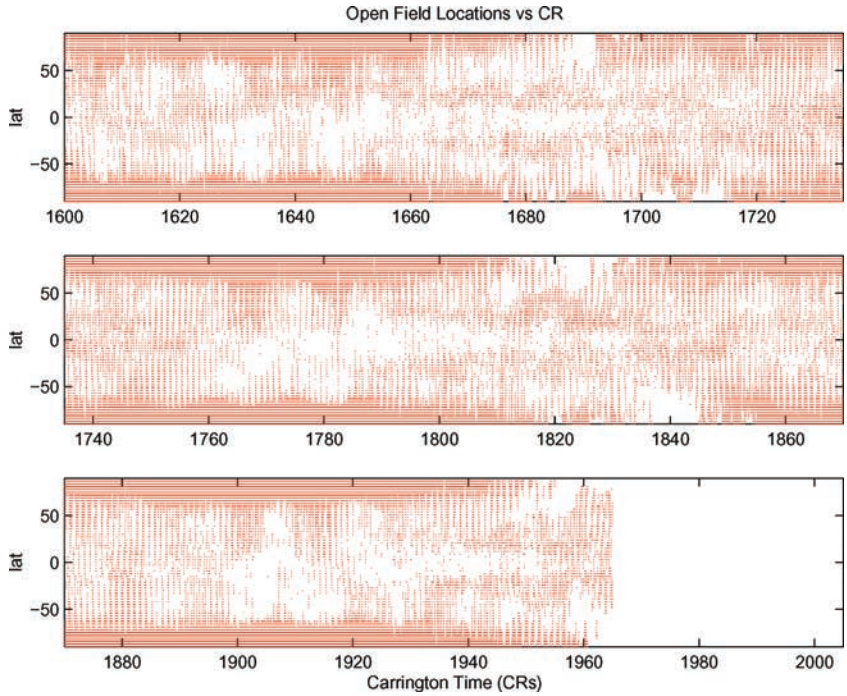

Figure 3. Photospheric foot points of coronal holes obtained from potential field source surface modeling for the period in Figure 2. Carrington time is, effectively, the central meridian location as time passes, as one scans across adjacent synoptic maps from right to left (time is reversed in synoptic maps). The polar holes can be seen as the dominant feature throughout much of the solar cycle, in part because of the latitude-longitude projection. They disappear only around solar maximum and not necessarily over the same period of time. The midlatitude and low-latitude holes essentially follow the appearance and disappearance of active regions. The active regions also produce polar hole extensions, which can last for many solar rotations. These are seen as nearly vertical repeating features that are ubiquitous throughout much of the solar cycle except around maximum.

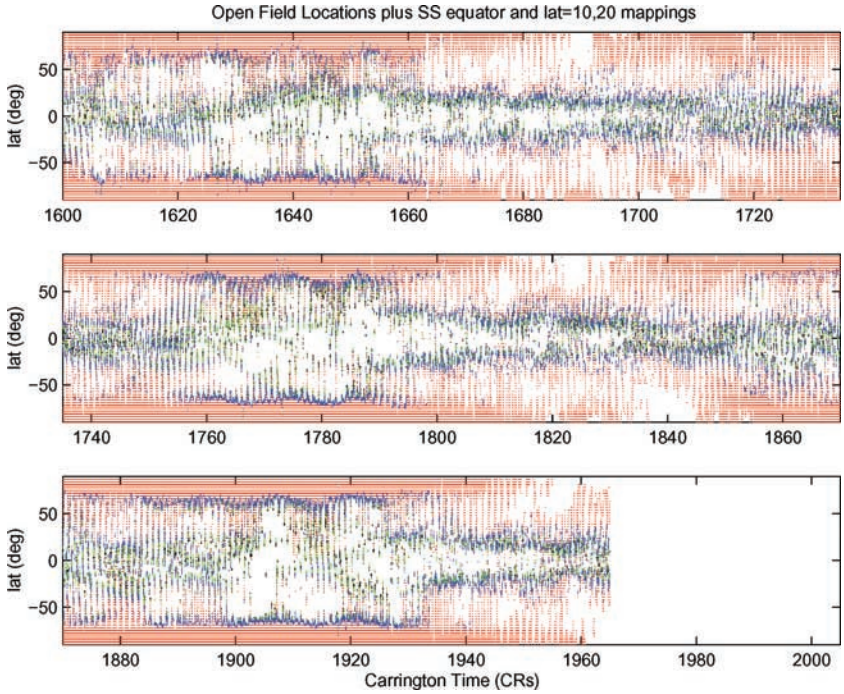

Figure 4. Foot points of coronal model field lines mapped to the photosphere from bands of starting points at 20° (blue), 10° (green), and 0° (black) on the source surface at 2.5 R_s. These foot points approximate the sources of the near-ecliptic solar wind through the solar activity cycles of Figure 1. The periods of polar hole source-dominated solar wind correspond to the periods of near-equatorial source surface neutral lines shown in Figure 3.

Northern Hemisphere polar hole vanishes before the Southern Hemisphere polar hole in both cycles 21 and 22. While the detailed shapes of the polar holes may be affected by our corrections to the polar regions of the synoptic maps described in section 3, the qualitative behavior is a robust feature of the solar cycles shown. Figure 3 also exhibits the ubiquitous coronal hole extensions as the persistent near-vertical stripes spaced at multiples of the Carrington rotation. The midlatitude and low-latitude isolated active region holes display the general behavior of the butterfly diagram, drifting from midlatitudes to low latitudes as the sunspot number rises to maximum then and declines.

[15] In Figure 4 the photospheric foot points of the PFSS model coronal field lines traced from 0° (black), 10° (green), and 20° (blue) north and south latitudes on the source surface are overlaid on the coronal holes to indicate the location(s) of the near-ecliptic solar wind sources (See Figures 1a–1c for the basic concept used here.) We consider that the 20° latitude span on either side of the source surface equator allows for the underestimated divergence of the polar coronal holes in the PFSS models (discussed by, e.g., *Wang* [1993]) as well as the solar rotation axis tilt with respect to the ecliptic. The evolution of the inferred low-heliolatitude solar wind sources from solar minimum to maximum shows the expected decrease of the polar hole contributions. However, this display suggests that the transition is rather abrupt and occurs about halfway into the cycle. The implication is that the active region coronal hole-dominated solar wind controls Earth's space environment during as much of the solar cycle as the polar hole solar wind. Moreover, at times when the active region coronal hole solar wind is dominant, the near-ecliptic solar wind is characterized by flows from a collection of smaller area distributed sources that diverge rapidly in the corona until they come into contact with streams from adjacent sources (e.g., as seen in Figure 1c).

[16] For the next displays we eliminate all of the coronal hole foot points except for those mapped from the low-latitude source surface, as seen in Figure 4. Figures 5a, 5b, and 5c, show the inferred magnetic polarity, magnetic field magnitude, and solar wind velocity for the sources implied by Figure 4. The field polarities and magnitudes are the photospheric values. In Figure 5a, red indicates outward radial fields, and blue indicates inward radial fields. In Figure 5b, red points are used for field magnitudes >30 G (on the smoothed map of the photospheric field), blue points for fields <10 G, and green is for intermediate values. The velocities in Figure 5c were obtained using the semiempirical approach developed by *Wang and Sheeley* [1990b], in which speed is related to PFSS model open flux tube divergence, with the modifications recently suggested by *Arge and Pizzo* [2000]. Red points indicate fast solar wind (here >550 km/s), blue points slow solar wind (<350 km/s), and green intermediate speed wind. Figure 6 shows the projected neutral line on the source surface for context.

[17] The magnetic field polarity plot in Figure 5a reinforces the paradigm of the simple sector structure from north and south polar coronal hole flows during the quiet

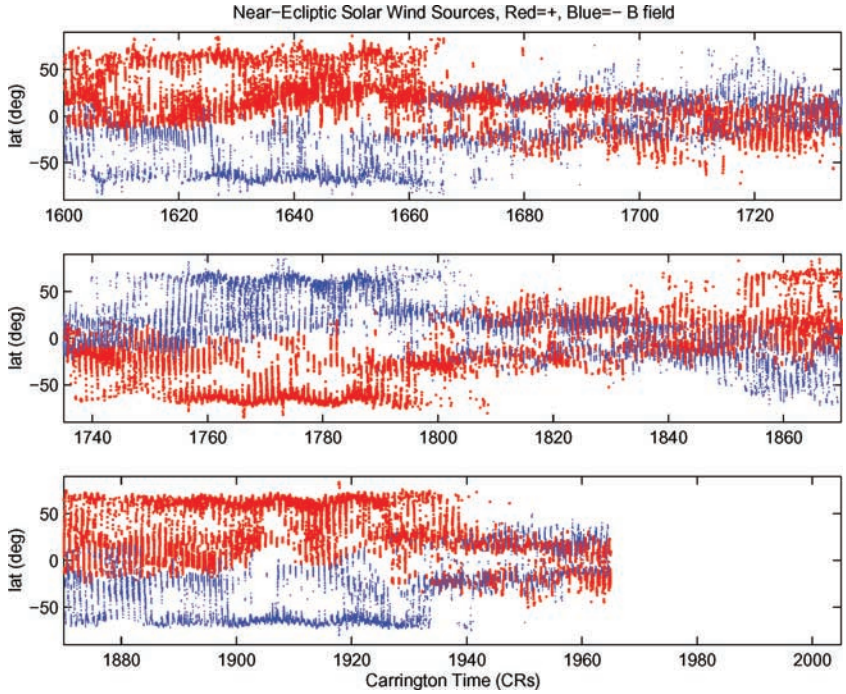

Figure 5a. Mapped foot points of Figure 4 from the low-latitude source surface, color-coded by photospheric magnetic field polarity. Red designates radially outward fields, and blue designates radially inward fields.

part of the cycle. However, over the period when the active region holes provide the low-latitude solar wind, there is a mix of polarities from a variety of low-latitude holes both north and south of the solar equator. Even though the polar coronal holes exist for ~85% of the solar cycle (see Figure 3), they do not organize the low-latitude interplanetary field for more than ~50% of the cycle. Moreover, the heliospheric neutral sheet, whose base is presumably the source surface neutral line (Figure 6), cannot generally be regarded as separating north and south

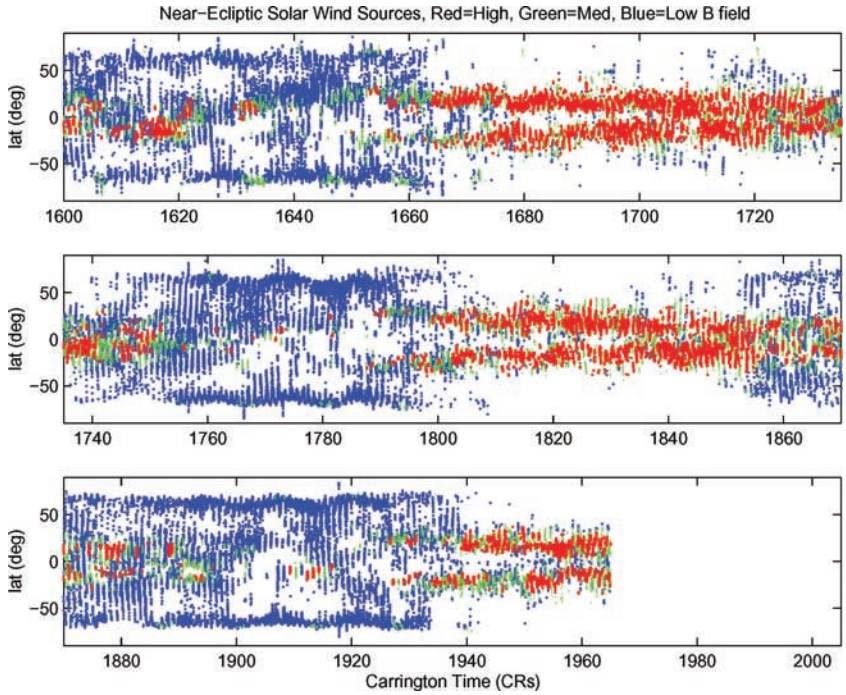

Figure 5b. Same as Figure 5a, but showing photospheric field strength at the foot points. Red designates strengths >30 G, blue designates strengths <10 G, and green denotes intermediate values.

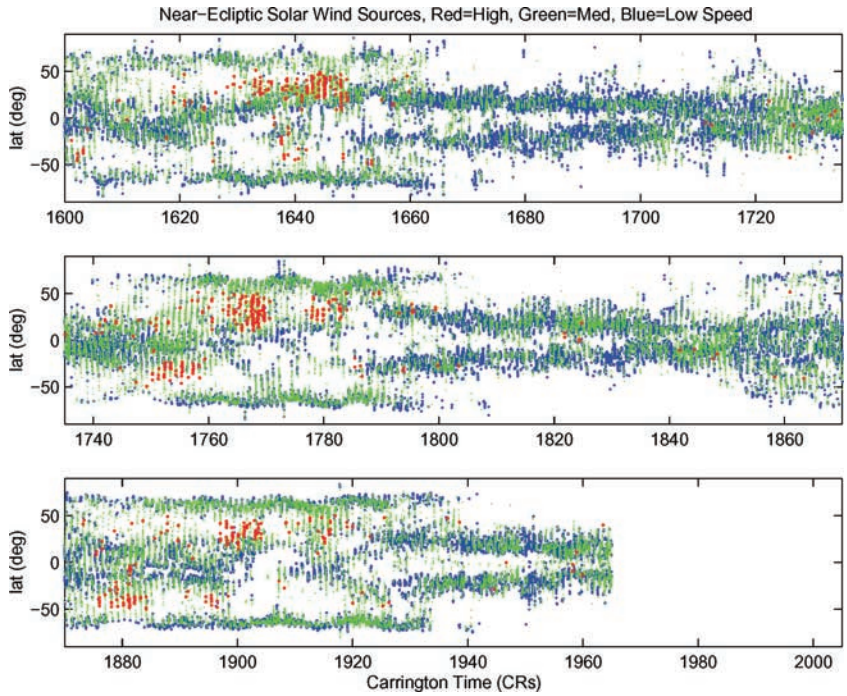

Figure 5c. Same as Figure 5b, but showing velocity of the solar wind associated with the open flux tube inferred using the *Wang and Sheeley* [1990b] flux tube divergence/velocity relationship as modified by *Arge and Pizzo* [2000]. Red designates inferred speeds >550 km/s, blue designates inferred speeds <350 km/s, and green denotes intermediate values.

polar coronal hole flows. Rather, it separates flows from holes with opposite magnetic polarity, including both polar and active region holes. Each solar wind magnetic sector thus typically arises from multiple sources. The inferred velocities in Figure 5c are consistent with previously obtained results where the lowest velocity or "slow" solar wind originates mainly from the low-latitude active region holes, while the highest velocities come from long polar

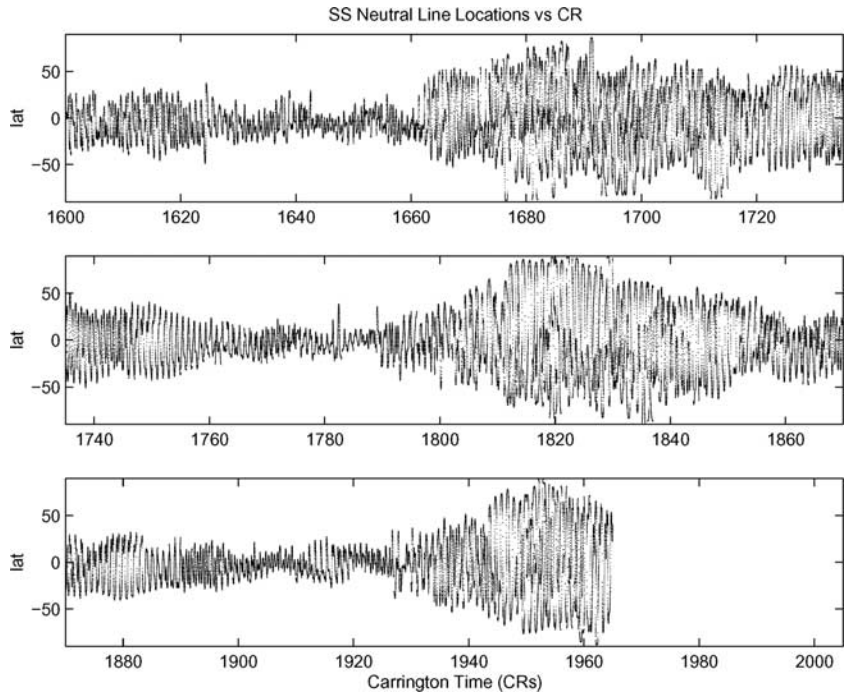

Figure 6. Record of the 2.5 R_s source surface (SS) neutral line for the period covered in Figures 1 and 2. Corresponding to the appearance of the active regions, the warp in the neutral line grows until the neutral line extends essentially from pole to pole around solar maximum.

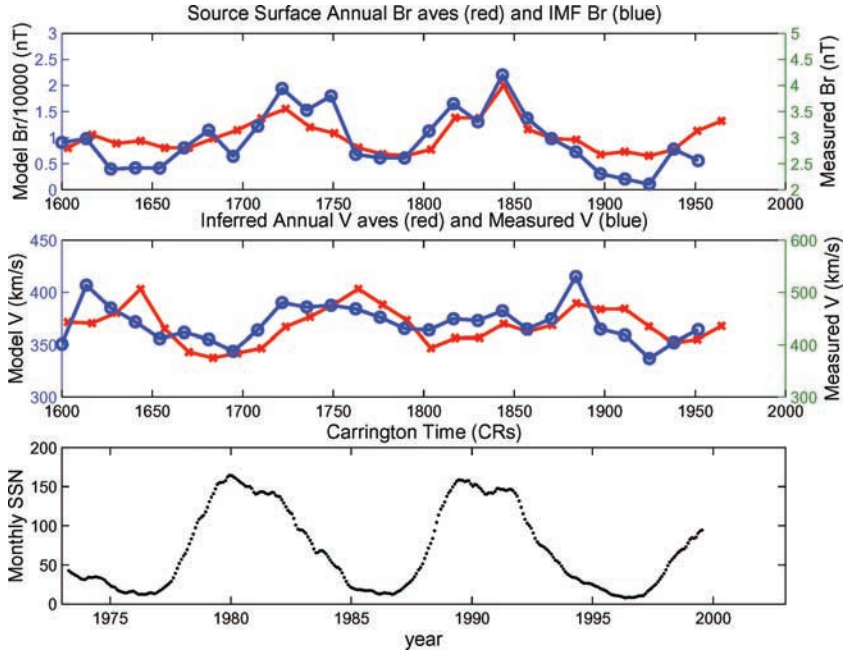

Figure 7. The annual average measured radial interplanetary magnetic field (top panel, blue curve) compares favorably in its general trend to the average (ave) radial field on the source surface (''model'' red curve). The units are 0.01 T for the source surface field and nanoteslas for the interplanetary field. The model velocities (in kilometers per second) in the center panel are computed for the low-latitude source surface using the *Wang and Sheeley* [1990b] approach but with the velocity dependence on flux tube expansion factor from *Arge and Pizzo* [2000]. Although the solar cycle is less evident in the model velocity, as well as in the corresponding annual measured velocities from the OMNI data, there is a tendency for velocity peaks to occur during the declining minimum phase, as previously noted.

coronal hole extensions [e.g., *Levine*, 1982; *Neugebauer et al.*, 1998].

5. Solar Wind and Space Weather Cycles

[18] From the displays in Figures 4–6 one expects to observe solar cycle behavior in key solar wind parameters like interplanetary magnetic field and velocity. In particular, Figure 5b suggests that the interplanetary magnetic field (IMF) should be stronger when the active region holes provide the major source, provided that the field divergence does not dilute the effect of this connection to the strong photospheric fields. The velocities in Figure 5c are inferred to have their maximum values in the period of the declining phase and solar minimum, out of phase with the larger fields.

[19] Figure 7 shows a complete time series, for the period of this study, of calculated annual averages of the radial magnetic field magnitude and inferred velocities at the source surface compared with corresponding values obtained from data in the OMNI archive [*King and Papitashvili*, 1994; *Gazis*, 1996]. The model radial fields are integrated over the source surface, given that Ulysses observations suggest the that IMF becomes uniform in latitude far from the Sun [*Forsyth et al.*, 1996]. The inferred velocities, in contrast, are based on values in the latitude band within 20° of the solar equator. The measured and modeled radial field agree in their cycle cadence and major features. We do not attempt to reproduce the interplanetary field magnitude here, as other authors [e.g., *Wang and Sheely*, 1988; *Wang*, 1993; *Zhao and Hoeksema*, 1995a, 1995b] have addressed the needed corrections due to the heliospheric current sheet mentioned in section 3. The model and measured velocities show similar trends in spite of the large scatter in the data used to determine the Wang and Sheeley empirical description of the local solar wind versus PFSS model flux tube divergence [*Wang et al.*, 1996], as well as our underestimates of the maximum field at the photosphere by use of a 17-order PFSS model (*Arge and Pizzo* [2000] used 30 orders to derive their improved formula). Neither model time series includes the effects of transient solar wind disturbances from CMEs, which are included in the OMNI data. The transient disturbance fields, e.g., from magnetic clouds and their surroundings, are not the primary cause of the observed solar cycle trends in the IMF strength [e.g., *Luhmann et al.*, 1993; *Richardson et al.*, 2001].

[20] The time series of CMEs can also be approximated from the PFSS model by calculating the average positive (only) derivatives of the CR source surface field magnitude time series, as was carried out by *Luhmann et al.* [1998]. (This approximation is considered reasonable if CMES do, in fact, represent newly opening coronal magnetic fields, as is suggested by their coronagraph image appearance as outward expanding loops or arcades. The newly opened field adds flux to the source surface, or to the interplanetary medium, in this view.) Figure 8 compares the modeled source surface field and velocity cycles with the annual averages of this derivative, superposed on the sunspot number. As was previously found [e.g., *Webb and Howard*,

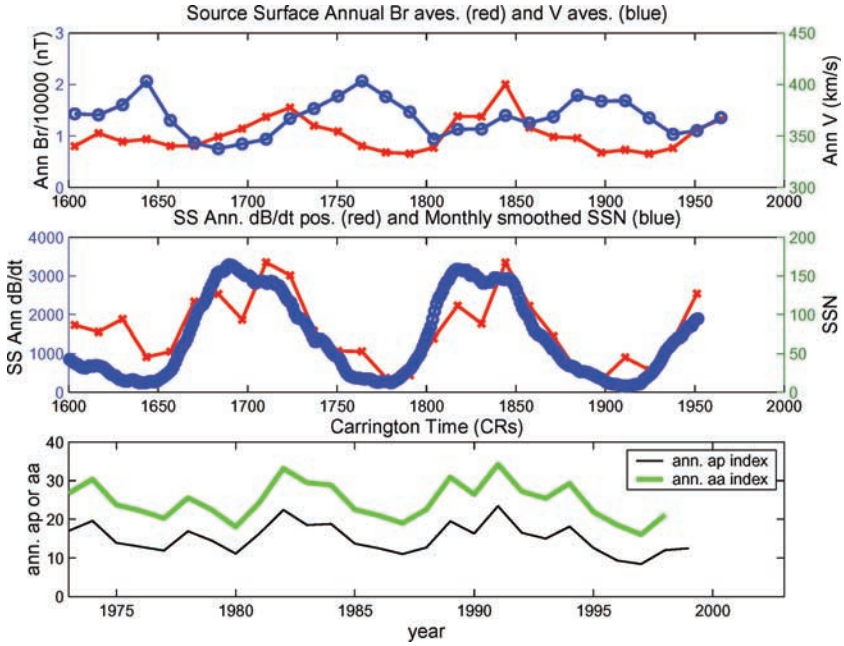

Figure 8. Cycles in the modeled solar wind field magnitude and velocity (top panel) and the approximate coronal mass ejection rate (middle panel, see section 5 for description), compared with the cycles in the *aa* and *ap* geomagnetic activity indices (bottom panel). The sunspot number is also shown in the middle panel for reference. The different interplanetary cycles can all affect the geomagnetic response, producing multiple peaks that may or may not have a unique interplanetary and solar connection.

1994], the inferred CME cycle generally follows the sunspot cycle, a behavior seen in the coronagraph observations of CMEs and in the counterstreaming interplanetary electron events associated with CME-initiated solar wind disturbances [*Gosling et al.*, 1992]. The double-peaked maximum in the inferred CME cycle is also of interest; however, the primary point made by Figure 8 is the three differently phased solar cycles of important solar wind and space weather parameters. The interplanetary magnetic field magnitude cycle coincides with the latter part of the sunspot maximum and declining phase when the total coronal hole area is greatest [*Wang*, 1993; *Wang et al.*, 2000], with active regions contributing to their fields. The solar wind velocity cycle shows a phase nearly opposite to that of the sunspot cycle and field magnitude cycle, with maxima where coronal hole extensions contribute high-speed streams to the low-latitude solar wind (see Figure 5c). The approximate CME cycle follows the sunspot cycle phase and exhibits double maxima. These different peaks in geoeffective quantities, produced by the solar activity cycle and related to the solar magnetic field evolution, must all affect space weather cycles to varying degrees. However, their effects are not necessarily independent.

[21] The bottom panel in Figure 8 displays the geomagnetic activity indices *aa* and *ap*, which also show cycles and peaks. The parameters controlling these have recently attracted fresh interest. In particular, *Stamper et al.* [1999] derived an empirical formula for the *aa* index in terms of solar wind parameters, including the IMF strength and solar wind velocity. These authors concluded that most of the trend in *aa* was due to IMF strength. However, some of the peaks in the annual averages of the *aa* index in Figure 8 seem to coincide with peaks in the inferred CME rates in the middle panel, and the peaks during the declining phase of the sunspot cycle are arguably related to velocity cycle peaks. Thus one must use caution when attributing trends observed in the geomagnetic indices to a single interplanetary parameter and solar origin (e.g., see *Feynman* [1982] and *Clilverd et al.* [1998] for several views on longer-term trends in geomagnetic indices). To truly unravel which quantity underlies the *aa* cycle and trends, it is necessary to distinguish magnetic storm (e.g., CME magnetic cloud) related increases in *aa* from the *aa* behavior outside of storm times [see *Richardson et al.*, 2001].

6. Discussion and Concluding Remarks

[22] The results presented above reinforce the idea that the contribution of polar coronal holes to the solar wind near the ecliptic is significant over only about half the solar cycle. The rest of the time the low-latitude solar wind is dominated by the flows from isolated low-latitude and midlatitude coronal holes or polar coronal hole extensions that have a flow character distinct from that of the large polar hole flows. The low-latitude holes and extensions significantly contribute even when the heliospheric current sheet is gently warped and is near equatorial. Thus the paradigm of a solar wind source consisting of two polar outflows flanking a planar current sheet, where the flow velocity has a minimum (e.g., as in the models of *Pizzo* [1982]), is atypical. A more realistic typical picture consists of two polar outflows separated at low latitudes by a number of independent unequal streams distributed around the solar equator. This multisource paradigm merits more routine consideration in both our interpretation of data upstream of Earth and in our

models of the solar wind streams and the propagation of coronal transients.

[23] Some consequences of a solar wind with an equatorial section of varying thickness composed of streams from multiple sources have already been reported in the literature. These include intervals of observed complex current sheet structures [e.g., *Crooker et al.*, 1993] and composition variations [e.g., *von Steiger*, 2000], suggesting contributions from a number of regions with different degrees of active region involvement, unlike the polar region streams that are rooted in the more uniform, magnetically quiet photosphere. Of course, the complexity of the slow solar wind produced by its multiple sources is in addition to complexity produced by the time dependence of the coronal hole geometries and photospheric properties. As pointed out before [*Wang and Sheeley*, 1990a], the emergence, submergence, or cancellation of photospheric flux, together with photospheric convection, field diffusion, and differential rotation, produce constantly changing coronal hole boundaries. Whether the change is radical (as in the disappearance or appearance of a mid-latitude or low-latitude hole), or evolutionary (as in the alteration of a coronal hole due to differential rotation of its defining photospheric sources) is immaterial. As both require some reconfiguration of the large-scale coronal field and its associated open field flow channels, they will appear as some transient form of solar wind that is detectable in interplanetary space [e.g., *Crooker et al.*, 1996]. These mix with the multistream source that affects us much of the time.

[24] The most general consequence of the changing sources of low-latitude solar wind is that cycles appear in the terrestrial response that are connected to the solar magnetic field behavior. The details of that connection are complicated and involve a number of ambient solar wind parameters as well as coronal transients. Thus it is necessary to carefully consider what each geomagnetic activity index physically means. For example, *Dst* is a good CME index, while *aa* and *ap* have greater contributions from auroral electrojets related to southward interplanetary fields in general. If it were possible to quantify the contributions of each kind of cycle in Figure 8, and other cycles such as solar EUV to geomagnetic indices, we would obtain a clearer perspective on the sources of space weather trends and their solar connections.

[25] **Acknowledgments.** This work was supported in part by NASA grant NAG5-7951 from the SEC Guest Investigator Program, and by NSF's Space Weather Program through a subcontract from Boston University.

[26] Hiroshi Matsumoto thanks I. G. Richardson and another referee for their assistance in evaluating this paper.

References

Altschuler, M. D., and G. Newkirk Jr., Magnetic fields and the structure of the solar corona, *Sol. Phys.*, *9*, 131, 1969.

Arge, C. N., and V. J. Pizzo, Improvement in the prediction of solar wind conditions using near-real time solar magnetic field updates, *J. Geophys. Res.*, *105*, 10,465, 2000.

Asai, K., M. Kojima, M. Tokumaru, A. Yokobe, B. V. Jackson, P. R. Hick, and P. K. Manoharan, Heliospheric tomography using interplanetary scintillation observations, 3, Correlation between speed and electron density fluctuations in the solar wind, *J. Geophys. Res.*, *103*, 1991, 1998.

Clilverd, M. A., T. D. G. Clark, E. Clarke, and H. Rishbeth, Increased magnetic storm activity from 1868 to 1995, *J. Atmos. Terr. Phys.*, *60*, 1047, 1998.

Crooker, N. U., G. L. Siscoe, S. Shodhan, D. F. Webb, J. T. Gosling, and E. J. Smith, Multiple heliospheric current sheets and coronal streamer belt dynamics, *J. Geophys. Res.*, *98*, 9371, 1993.

Crooker, N. U., M. E. Burton, J. L. Phillips, E. J. Smith, and A. Balogh, Heliospheric plasma sheets as small scale transients, *J. Geophys. Res.*, *101*, 2467, 1996.

Feynman, J., Geomagnetic and solar wind cycles, 1900–1975, *J. Geophys. Res.*, *87*, 6153, 1982.

Forsyth, R. J., A. Balogh, T. Horbury, G. Erdös, E. Smith, and M. Burton, The heliospheric magnetic field at solar minimum: Ulysses observations from pole to pole, *Astron. Astrophys.*, *316*, 287, 1996.

Gazis, P. R., Solar cycle variation in the heliosphere, *Rev. Geophys.*, *34*, 379, 1996.

Gosling, J. T., D. J. McComas, J. L. Phillips, and S. J. Bame, Counterstreaming solar wind electron events: Solar cycle variations, *J. Geophys. Res.*, *97*, 6531, 1992.

Hoeksema, J. T., J. M. Wilcox, and P. H. Scherrer, Structure of the heliospheric current sheet: 1978–1982, *J. Geophys. Res.*, *88*, 9910, 1983.

King, J. H., and N. E. Papitashvili, *Interplanetary Medium Data Book, Supplement 5, 1988–1993, NSSDC/WDC-A-R&S 94-08*, NASA/NSSDC/GSFC, Greenbelt, Md., 1994.

Kojima, M., T. Fujiki, M. Ohmi, M. Tokumaru, and A. Yokobe, Low-speed solar wind from the vicinity of active regions, *J. Geophys. Res.*, *104*, 16,993, 1999.

Levine, R. H., The relation of open magnetic structures to solar wind flow, *J. Geophys. Res.*, *83*, 4193, 1978.

Levine, R. H., Open magnetic fields and the solar cycle, I, Photospheric sources of open magnetic flux, *Sol. Phys.*, *79*, 203, 1982.

Levine, R. H., M. Schulz, and E. N. Frazier, Simulation of the magnetic structure of the inner heliosphere by means of a nonspherical source surface, *Sol. Phys.*, *77*, 363, 1982.

Lockwood, M., R. Stamper, and M. N. Wild, A doubling of the Sun's coronal magnetic field during the last 100 years, *Nature*, *399*, 437, 1999.

Luhmann, J. G., T. L. Zhang, S. M. Petrinec, C. T. Russell, P. Gazis, and A. Barnes, Solar cycle 21 effects on the interplanetary magnetic field and related parameters at 0.7 and 1.0 AU, *J. Geophys. Res.*, *98*, 5559, 1993.

Luhmann, J. G., J. T. Gosling, J. T. Hoeksema, and X. Zhao, The relationship between large-scale solar magnetic field evolution and coronal mass ejections, *J. Geophys. Res.*, *103*, 6585, 1998.

McComas, D. J., B. L. Barraclough, H. O. Funsten, J. T. Gosling, E. Santiago-Munoz, R. M. Skoug, B. E. Goldstein, M. Neugebauer, P. Riley, and A. Balogh, Solar wind observation over Ulysses' first full polar orbit, *J. Geophys. Res.*, *105*, 10,419, 2000.

Neugebauer, M., et al., Spatial structure of the solar wind and comparisons with solar data and models, *J. Geophys. Res.*, *103*, 14,587, 1998.

Odstrcil, D., and V. J. Pizzo, Distortion of the interplanetary magnetic field by three-dimensional propagation of coronal mass ejections in a structured solar wind, *J. Geophys. Res.*, *104*, 28,225, 1999.

Pizzo, V. J., A three-dimensional model of corotating streams in the solar wind III Magnetohydrodynamic streams, *J. Geophys. Res.*, *87*, 4374, 1982.

Richardson, I. G., E. W. Cliver, and H. V. Cane, Sources of geomagnetic storms for solar minimum and maximum conditions during 1972–2000, *Geophys. Res. Lett.*, *28*, 2569, 2001.

Riley, P., J. T. Gosling, and V. J. Pizzo, A two-dimensional simulation of the radial and latitudinal evolution of a solar wind disturbance driven by a fast, high pressure, coronal mass ejection, *J. Geophys. Res.*, *102*, 14,677, 1997.

Schatten, K. H., J. M. Wilcox, and N. F. Ness, A model of interplanetary and coronal magnetic fields, *Sol. Phys.*, *6*, 442, 1969.

Schulz, M., Non-spherical source-surface model of the heliosphere: A scalar formulation, *Ann. Geophys.*, *15*, 1379, 1997.

Sheeley, N. R., Jr., J. H. Walters, Y.-M. Wang, and R. A. Howard, Continuous tracking of coronal outflows: Two kinds of coronal mass ejections, *J. Geophys. Res.*, *104*, 24,739, 1999.

Stamper, R., M. Lockwood, M. N. Wild, and T. D. G. Clark, Solar causes of the long-term increase in geomagnetic activity, *J. Geophys. Res.*, *104*, 28,325, 1999.

Ulrich, R. K., Analysis of magnetic flux tubes on the solar surface from observations at Mt. Wilson of l5250 and l5233, in *Cool Stars, Stellar Systems, and the Sun*, edited by M. S. Giampapa and J. A. Bookbinder, p. 265, Astron. Soc. of the Pac., San Francisco, Calif., 1992.

von Steiger, R., et al., Composition of quasistationary solar wind flows from Ulysses solar wind ion composition spectrometer, *J. Geophys. Res.*, *105*, 27,217, 2000.

Wang, Y.-M., On the latitude and solar cycle dependence of the interplanetary magnetic field strength, *J. Geophys. Res.*, *98*, 3529, 1993.

Wang, Y.-M., and N.-R. Sheeley Jr., The solar origin of long-term variations of the interplanetary magnetic field strength, *J. Geophys. Res.*, *93*, 11,227, 1988.

Wang, Y.-M., and N. R. Sheeley Jr., Magnetic flux transport and the sunspot cycle evolution of coronal holes and their wind streams, *Astrophys. J.*, *365*, 372, 1990a.

Wang, Y.-M., and N. R. Sheeley Jr., Solar wind speed and coronal flux tube expansion, *Astrophys. J.*, *355*, 726, 1990b.

Wang, Y.-M., and N. R. Sheeley Jr., On potential field models of the solar corona, *Astrophys. J.*, *292*, 310, 1992.

Wang, Y.-M., and N. R. Sheeley Jr., Global evolution of interplanetary sector structure, coronal holes, and solar wind streams during 1976–1993: Stackplot displays based on solar magnetic field observations, *J. Geophys. Res.*, *99*, 6597, 1994.

Wang, Y.-M., and N. R. Sheeley Jr., Solar implications of ULYSSES interplanetary field measurements, *Astrophys. J.*, *447*, L143, 1995.

Wang, Y.-M., S. H. Hawley, and N. R. Sheeley Jr., The magnetic nature of coronal holes, *Science*, *271*, 464, 1996.

Wang, Y.-M., J. Lean, and N. R. Sheeley Jr., The long-term variation of the Sun's open magnetic flux, *Geophys. Res. Lett.*, *27*, 505, 2000.

Webb, D. F., and R. A. Howard, The solar cycle variation of coronal mass ejections and the solar wind mass flux, *J. Geophys. Res.*, *99*, 4201, 1994.

Zhao, X.-P., and J. T. Hoeksema, Prediction of the interplanetary magnetic field strength, *J. Geophys. Res.*, *100*, 19, 1995a.

Zhao, X.-P., and J. T. Hoeksema, Modeling the out of ecliptic interplanetary magnetic field in the declining phase of sunspot cycle 22, *Space Sci. Rev.*, *72*, 189, 1995b.

Zhao, X.-P., and A. Hundhausen, Organization of solar wind plasma properties in a tilted, heliomagnetic coordinate system, *J. Geophys. Res.*, *86*, 5423, 1981.

C. N. Arge, NOAA Space Environment Center, 325 Broadway, Boulder, CO 80303, USA. (nick.arge@noaa.gov)

P. R. Gazis, NASA Ames Research Center, MS 245-3, Moffet Field, CA 94035, USA. (pgazis@mail.arc.nasa.gov)

Y. Li and J. G. Luhmann, Space Sciences Laboratory, University of California, Berkeley, CA 94720, USA. (yanli@ssl.berkeley.edu; jgluhmann@ssl.berkeley.edu)

R. Ulrich, Department of Physics and Astronomy, University of California, Los Angeles, CA 90095, USA. (Ulrich@astro.ucla.edu)